Geometry and time scales of self-consistent orbits in a modified SU(2) model

D. M. Jezek, E. S. Hernández, and H. G. Solari
Departamento de Física, Facultad de Ciencias Exactas y Naturales, Universidad de Buenos Aires, 1428 Buenos Aires, Argentina
(Received 20 May 1985)

We investigate the time-dependent Hartree-Fock flow pattern of a two-level many fermion system interacting via a two-body interaction which does not preserve the parity symmetry of standard SU(2) models. The geometrical features of the time-dependent Hartree-Fock energy surface are analyzed and a phase instability is clearly recognized. The time evolution of one-body observables along self-consistent and exact trajectories are examined together with the overlaps between both orbits. Typical time scales for the determinantal motion can be set and the validity of the time-dependent Hartree-Fock approach in the various regions of quasispin phase space is discussed.

I. INTRODUCTION

The time-dependent-Hartree-Fock (TDHF) method has become popular in the nuclear physics literature due to its microscopic characteristics and its moderately large amount of computational requirements as long as simplified effective interactions are employed.[1-6] Insofar as its validity was shown to be restricted to short times[7] or to very large particle numbers,[8,9] the method is related to an asymptotic expansion. It appears clear that the major confidence may be put on its ability to describe the large amplitude collective motion of a heavy nucleus.

Physical interest and computation feasibility have pushed TDHF calculations through the whole Periodic Table, with particularly striking results, such as the appearance of a low angular momentum window for fusion[2] and the serious rotational symmetry breaking for light nuclides.[10] These situations require that the nature and abilities of the TDHF approach should be examined, keeping in mind the possibilities of establishing rules and criteria for a safe utilization of the approach. This kind of work is partially supported by the study of solvable nontrivial systems, which allow the comparison between approximate and exact dynamics.[11-13]

Among the consistency criteria sought for, the time of validity of the TDHF approach in terms of the residual interaction has been analyzed by Lichtner and Griffin.[7] Unfortunately, the evaluation of this parameter demands a large amount of calculation, and it is not possible to discriminate between the relative roles of excited and unexcited configurations. In this way one can only expect to get a lower limit of validity of the TDHF method. Another criterion of consistency recently suggested appeals to known features of the exact dynamics such as symmetries[10,13] and a method has been proposed[13,14] that overcomes one of the most important drawbacks of the self-consistent dynamics, namely its restriction to short times. In this approach—that we have called symmetry conserving variational dynamics (SCVD)—one takes fundamental advantage of the existing symmetries in order to propose, as a variational trial wave function, a superposition of Slater determinants selected so as to guarantee the conservation of the group symmetry operator. It has been shown[13] in the frame of the standard SU(2) model[15] that such a wave function evolves in time according to a nonlinear equation of motion on the Grassmann manifold and offers a much better resemblance to the exact one, over a longer time interval than the single TDHF determinant.

Since the criteria resting on symmetry arguments may establish necessary conditions controlling some specific degrees of freedom,[14] it seems interesting to investigate systems which do not present symmetries (or the set of degrees of freedom not related to the existing symmetries) in order to get a better understanding of the qualities and abilities of the TDHF method when it is applied far from its asymptotic zone of primary validity. For such systems or coordinates, there is not any obvious key to the construction of an improved variational wave function as in the SCVD case. This situation suggests the convenience of a detailed study of the TDHF orbits, looking for those regularities of the mean field flow that might indicate correlations whose explicit inclusion—like the conserved observables in the SCVD approach—could make room to a better representation of the exact wave function. For this purpose, in this work we propose, among many other possibilities that we defer to a future work,[16] a particular SU(2) model where the parity symmetry is missing, and perform an analysis of the TDHF flow pattern that permits to extract some systematic features of the figures that may quantitatively indicate the good or poor quality of the approach. For this sake, in Sec. II we present the model and establish a method of construction of the TDHF phase portrait that consists of projecting the energy surface on the Bloch sphere, while in Sec. III a comparison between TDHF and the exact dynamics is performed through various kinds of estimates like overlaps and mean values of one-body observables. The last section (Sec. IV) is reserved for the conclusions.

II. GEOMETRY OF THE TDHF ENERGY SURFACES

The pattern of the TDHF dynamics of r-level systems is very closely related to the geodesic flow on a sphere in a $(2r-1)$-dimensional space,[17] since the Slater deter-

minants may be set into a one-to-one correspondence with the coherent states of the SU(r) group. In particular, the correspondence between two-level systems and quasispin models has been widely utilized in the past.[11–13,15,18–20]

We are going to analyze the TDHF dynamics induced by the one- and- two-body Hamiltonian,

$$\hat{H}=\epsilon\hat{J}_z+\frac{v}{2}(\{\hat{J}_+\hat{J}_z\}+\{\hat{J}_-\hat{J}_z\})$$
$$=\epsilon\hat{J}_z+v\{\hat{J}_x\hat{J}_z\}\ , \tag{2.1}$$

in a two-level system, where

$$\hat{J}_z=\tfrac{1}{2}\sum_{P,\sigma=\pm1}\sigma a^+_{P\sigma}a_{P\sigma}\ , \tag{2.2a}$$

$$\hat{J}_+=\sum_P a^\dagger_{P\sigma}a_{P,-\sigma}=(\hat{J}_-)^\dagger\ , \tag{2.2b}$$

are the components of the quasispin vector $\hat{\mathbf{J}}$ expanding the SU(2) Lie algebra, the symbol $\{\ \}$ is the usual anticommutator and $a^\dagger a$ are the single-particle creation and annihilation operators.

One should notice that opposite to the standard Lipkin model,[15] in which the two-body interaction scatters a pair of particles from one level into the other, the Hamiltonian (2.1) does not commute with the parity operator $\hat{P}=e^{i\pi\hat{J}_z}$. The latter property is due to the fact that the interaction (2.1) allows odd numbers of particle-hole excitations to couple to even-numbered ones. The structure of the present Hamiltonian is more suitable for a rough model of particle transfer between nuclei in a collision, as it is schematically indicated in Fig. 1.

The set of Slater determinants which may be generated out of the unperturbed ground state by operations of the SU(2) group are of the form[12,13,21,22]

$$|\tau\rangle=\hat{R}(\tau)|-J,J\rangle\ , \tag{2.3}$$

where $\hat{R}(\tau)$ is the rotation operator,

$$\hat{R}(\tau)=(1+|\tau|^2)^{-J}\exp(\tau\hat{J}_\dagger-\tau^*\hat{J}_-)\ , \tag{2.4}$$

and $|-J,J\rangle$ is the unperturbed ground state, where $J=N/2$ labels the fully symmetric representation of the rotation group.

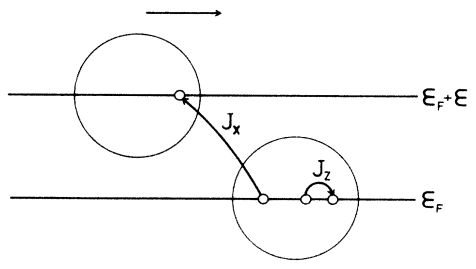

FIG. 1. Schematic representation of a nucleus-nucleus collision with particle transfer. The Fermi energy ϵ_F is proportional to the average energy per particle in each nucleus and the projectile posesses an excess energy ϵ. The quasispin projection $\hat{J}_x$ is related to the transfer process, while $\hat{J}_z$ simply provides diagonal-like scattering.

The complex parameter τ is related to real parameters (θ,φ) that represent angles on the Bloch sphere or manifold of the SU(2) coherent states, through the expression

$$\tau=\tan\left[\frac{\theta}{2}\right]\exp(-i\varphi)\ , \tag{2.5}$$

and in terms of these variables the mean values of the one-body observables $\hat{J}_x$, $\hat{J}_y$, and $\hat{J}_z$, namely the Cartesian components of the quasispin $\hat{\mathbf{J}}$, with respect to the collective state $|\tau\rangle$, read

$$\langle\hat{J}_x\rangle=J\sin\theta\cos\varphi\ , \tag{2.6a}$$

$$\langle\hat{J}_y\rangle=J\sin\theta\sin\varphi\ , \tag{2.6b}$$

$$\langle\hat{J}_z\rangle=J\cos\theta\ . \tag{2.6c}$$

Hereafter, we will utilize the notation $\mathcal{O}=\langle\tau|\hat{\mathcal{O}}|\tau\rangle$ for the expectation values of operators.

The TDHF dynamics is imposed upon the system by resorting to Dirac's variational principle,[23]

$$\delta\int dt\left\langle\tau\left|i\hbar\frac{\hat{\partial}}{\partial t}-\hat{H}\right|\tau\right\rangle=0\ , \tag{2.7}$$

with $|\tau\rangle$ lying on the manifold of determinants. The Euler-Lagrange equations of motion are Hamiltonian[13,18,24,25] and adopt the canonical form when written in the representation $q=\varphi$ and $p=-J\cos\theta$, namely,

$$\dot{q}=\partial\mathcal{H}/\partial p\ , \tag{2.8a}$$

$$\dot{p}=-\partial\mathcal{H}/\partial q\ , \tag{2.8b}$$

the classical Hamiltonian being the expectation value on the Grassmann manifold,

$$\mathcal{H}=\langle\tau|\hat{H}|\tau\rangle\ . \tag{2.9}$$

For the quantal Hamiltonian (2.1), we obtain,

$$\mathcal{H}=\epsilon J\left[-\cos\theta-\frac{\chi}{2}\sin2\theta\cos\varphi\right]\ ,\quad \chi=\frac{v(N-1)}{\epsilon}\ , \tag{2.10}$$

and the equations of motion (2.8) can be written as

$$\dot{\varphi}=\frac{\epsilon}{\sin\theta}(\sin\theta-\chi\cos\varphi\cos2\theta)\ , \tag{2.11a}$$

$$\dot{\theta}=\epsilon\chi\sin\varphi\cos\theta\ . \tag{2.11b}$$

On the other hand, one can demonstrate that the dynamics arising from (2.7)—that geometrically represents the motion of the "tip" of the vector $\mathbf{J}$ on the Bloch sphere—can be viewed as a generalized goedesic flow[26] with local angular velocity $\boldsymbol{\omega}=\nabla_J\mathcal{H}$, namely,

$$\frac{d\mathbf{J}}{dt}=\nabla_J\mathcal{H}\times\mathbf{J}\ , \tag{2.12}$$

with $\times$ denoting vector or external product.

Equation (2.12) is the statement of Ehrenfest's theorem when the state under consideration is a Slater determinant, simply meaning that the velocity $d\mathbf{J}/dt$ agrees

with the exact one whenever the exact state touches the Bloch sphere. This equation also reflects the restriction of the trajectory to lie on the Grassmann manifold, since the external product operation forces the vector **J**—hereafter to be named the "polarization" vector—to remain on the Bloch sphere $|\mathbf{J}|=cte$. On the other hand, Eq. (2.12) ensures energy conservation, the energy for each trajectory being the expectation value (2.10). One can show that the consistency of the dynamics with both manifold invariance and energy conservation is valid in general, thus Eq. (2.12) might be extended to systems with higher number of levels. In any case, the intersection of a given energy surface $\mathscr{H}=cte$, $\mathscr{H}$ given by Eq. (2.9), with the Grassmann or coherent state manifold for the group under consideration, determines the submanifold where the motion takes place.

In the situation here considered, restrictions $|\mathbf{J}|=cte$ and $\mathscr{H}=cte$ together determine the path along which the motion occurs. Indeed, being both invariant manifolds two-dimensional surfaces, their intersection is a curve. Moreover, as long as we restrict ourselves to quadratic (two-body interaction) Hamiltonians, both the energy surface and the Grassmann manifold are just quadrics in the quasispin variables, namely

$$\mathbf{J}\cdot\mathbf{J}=J^2\,, \tag{2.13a}$$

$$\mathscr{H}=\epsilon J_z\left[J_x+\frac{J}{\chi}\right]\,. \tag{2.13b}$$

The latter represents a hyperbolic cylinder centered at $(-J/\chi,0,0)$ and with axial symmetry with respect to the J_y axis.

The flow pattern changes with the interaction strength. As χ scales from zero to infinity the center of the hyperbolic cylinder (2.13b) moves from minus or plus infinity to zero along the J_x axis, reaching a critical point for $\chi=\pm 1$ when this central point enters the Bloch sphere. This situation represents a qualitative change in the shape of the orbits and in the case of the standard SU(2) model[15] it has been referred to as a phase transition.[18] It is worthwhile noticing that in the present case a transition of the phase flow from one to another morphology takes place, rather than a ground-state phase transition as in the well-known Lipkin model.[12,15,18] In fact, a calculation of the critical points of the energy surface (2.10) indicates that the absolute minimum continuously moves upwards from the south pole ($\chi=0$) to the point $\theta=\pi/4$, $\varphi=0$ ($\chi\to\infty$), without any bifurcation appearing. It is possible, however, a qualitative analysis of the evolution of every critical point, by inspection of Fig. 2, where the relative location of the maxima and minima of the energy surface—i.e., the fixed points of the flow—is illustrated for the whole range of interaction strengths. The above-mentioned transition of the flow becomes then clearly displayed and hereafter we will refer to it as a catastrophe or structural instability, with the meaning of a "transition-in-phase," with the understanding that this is not a thermodynamic phase transition.

In this figure, we can appreciate that for weak interactions the energy surfaces are very close to planes in the region where the Bloch sphere lies. Then, most motions are

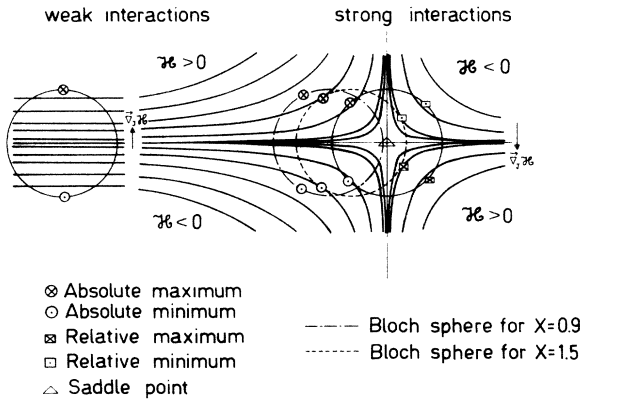

FIG. 2. The flow pattern on the Bloch sphere for various interaction strengths χ. Orbits on the manifold of Slater determinants are the intersections between the latter and the energy hyperbolic cylinders $\mathscr{H}=cte$.

rotations with a nearly constant angular velocity. Whatever the value of $|\chi|$, there are two stationary points of the energy surface, a maximum and a minimum located at the north and south hemispheres, respectively. These fixed points depart from the corresponding poles when the interaction strength departs from zero and move towards the equator along the $\varphi=0$ meridian as $|\chi|$ increases. The z component of the local angular velocity is always positive (negative) if χ remains smaller than unity (larger than -1), implying that there is a unique flow direction on the sphere. In addition, there is a one-to-one correspondence between energies and trajectories and the time required to travel around the equator is finite:

$$T_{\rm eq}=\int_0^{2\pi}\frac{d\varphi}{\epsilon(1+\chi\cos\varphi)}=\frac{2\pi}{\epsilon\sqrt{1-\chi^2}}\,. \tag{2.14}$$

Notice, however, that two separatrices appear for any nonvanishing coupling strength; these are the two orbits containing the poles with energies $\pm\epsilon J$, the plus (minus) sign corresponding to the trajectory through the north (south) pole. Each of these separates the region of closed orbits around the local extremum from the region of rotations covering most of the Bloch sphere. The flow pattern for $\chi=0.9$ is illustrated in Fig. 3.

The case of strong interactions ($|\chi|>1$) substantially

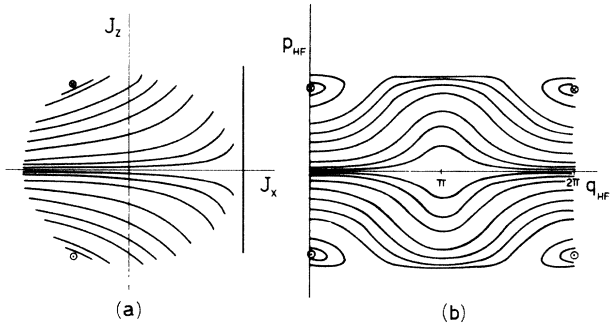

FIG. 3. The flow pattern for $\chi=0.9$ (a) on the Bloch sphere (b) on the HF phase space $(p_{\rm HF},q_{\rm HF})$. The extrema are indicated with the symbols displayed in Fig. 2.

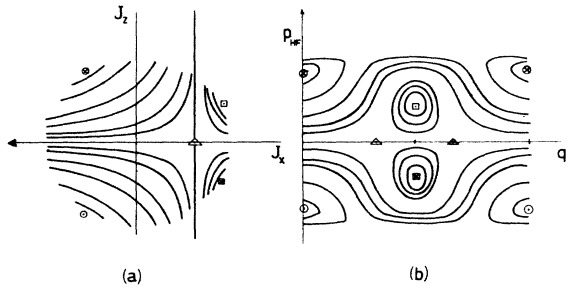

FIG. 4. Same as in Fig. 3, for an interaction strength $\chi=1.5$. The asymptotic plane separates the ordinary zone ($\omega_z>0$) on the left half-space from the extraordinary one where $\omega_z<0$.

differs from the situation with $|\chi|<1$. When the intersection parameter crosses the critical value $|\chi_c|=1$ the phase portrait presents two topologically distinct sets of orbits, the one resembling the weak-interaction pattern with librations around the local extrema and rotations on the rest of the sphere, the other containing only librations, symmetrically located with respect to the equator. A typical pattern for $\chi=1.5$ is shown in Fig. 4.

By inspection of this figure we realize that the bifurcation gives rise to a pair of relative maxima and minima lying on the meridian $\varphi=\pi$ while the absolute extrema remain on the $\varphi=0$ meridian. These relative extrema bifurcate from a saddle point on the equator that appears when the asymptotic plane of the hyperbolae becomes tangent to the sphere for $|\chi|=1$. Indeed, the saddle point suffers a fourfold bifurcation, since in addition to the extrema that evolve along the meridian $\varphi=\pi$, two new saddle points depart and remain on the equatorial line (see Fig. 4). In the limit where χ approaches infinity, both the relative and the absolute extrema at a given hemisphere coincide on the midparallel $\theta=\pi/4$ or $3\pi/4$ (cf. Fig. 2). We observe that the intersection of the plane $J_x=-J/\chi$ and the Bloch sphere is the separatrix between the new sets of librations and the previously existing rotations and librations. Hereafter, we will denote these invariant sets as the ordinary (or regular) and the extraordinary (or exceptional) zones, the former containing the librations around the absolute extrema and the rotations, the latter, the librations around the relative extrema. In addition, one can verify that the z component of the angular velocity $\omega=\nabla_J\mathscr{H}$ changes sign from one to the other region. Furthermore, all energies in the interval between the relative extrema are degenerate, since there exist orbits with the same energy in the regular zone.

Finally, we point out that after the catastrophe has occurred the equatorial orbit becomes a separatrix as well. This is due to the appearance of two saddle points at $J_x=-J/\chi$, which assigns an infinite period to the trajectory containing them.

III. NUMERICAL STUDY

We are interested in comparing the exact dynamics represented by the Schrödinger equation,

$$i\hbar\dot{a}_n=\sum_{j=0}^{N}\langle n|\hat{H}|n+j\rangle a_{n+j}\ ,\quad 0\le n\le N\ , \tag{3.1}$$

where $|n\rangle$ are the $(2J+1)$ vectors of the Dicke basis, and the TDHF evolution given by

$$i\hbar\dot{\tau}=\epsilon\left[\tau+\chi\frac{3\tau^2+3|\tau|^2-\tau^2|\tau|^2-1}{2(1+|\tau|^2)}\right]\ . \tag{3.2}$$

Equation (3.2) is the complex version of the real canonical equations (2.11). This comparison can be done through a set of indicators, such as the overlap between the exact and the TDHF state vectors $|E\rangle$ and $|\tau\rangle$, respectively, and the expectation values of the one-body observables in both dynamics. In what follows, the situation is analyzed in the framework of either weak or strong interactions, founding the discussion on the characteristics of the orbits.

A. Weak interactions

For ordinary librations close to either extremum we can observe a high correlation between exact and approximate polarization vectors as shown in Fig. 5 for a coupling strength $\chi=0.9$, as well as the values of the overlap $\langle E|\tau\rangle$ remaining very close to the unity. In agreement with the last observation we realize that the modulus of the exact polarization $\mathbf{J}_E$ mostly stays in a narrow shell close to surface of the Bloch sphere.

When the initial conditions are selected on orbits lying farther from the extrema, the exact polarization moves in a wider region and penetrates deeper into the Bloch sphere. This is clearly displayed in Fig. 5 for four different orbits, whose initial positions are $\theta=0.75\pi$, 0.66π, 0.6π, and 0.52π along the $\varphi=0$ meridian. These initial conditions range from the critical point to the equator covering the θ interval where significant variations in the shape of the polarization curves can be observed. Values of θ_0 higher than 0.75π yield almost horizontal curves; in other words, the exact polarization performs very small amplitude excursions in the vicinity of the critical point. When θ_0 equals the location of the maximum $\theta_M=0.84\pi$, the exact trajectory is practically the fixed point. Accordingly, we have verified that the overlap decreases in a significant fashion (even up to a 15% figure) as the exact polarization departs from the surface of the sphere.

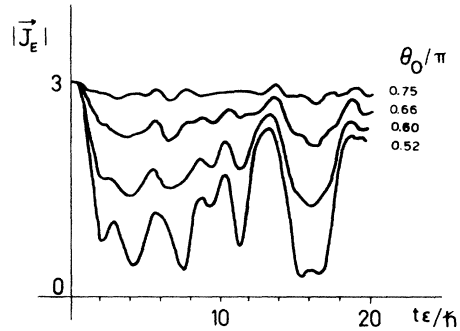

FIG. 5. The modulus of the exact polarization vector $\mathbf{J}$ as a function of time for $N=6$ and $\chi=0.9$. The numbers θ_0/π denote the initial positions on the $\varphi=0$ meridian and belong to the ordinary zone of the HF phase space.

In Fig. 5 we may as well notice that the vector $\mathbf{J}_E$ approaches the surface of the sphere after an elapsed time of about $14.5\hbar/\epsilon$, with independence of the initial conditions. The TDHF calculation makes evident that this encounter occurs at a point close to the same self-consistent orbit where that motion started. On the other hand, we have numerically computed the TDHF period of the displayed orbits and found that they vary between 0.66 and 14.4 $\hbar/\epsilon$ for the same initial conditions. Since the apparent recursion times of the exact orbits in Fig. 5 do not exhibit the important variations of the periods of the TDHF ones, we can in principle disregard the hypothesis of a high correlation between those different motions and presume in this case that in the exact dynamics the TDHF component is mostly decoupled from the component driving the motion towards the interior of the sphere.

B. Strong interactions

1. Ordinary zone

The investigation of the exact orbits in the neighborhood of the absolute extrema leads to observations analogous to those mentioned in the weak interaction case, namely a good agreement between exact and approximate paths. The polarization vectors are exhibited in Fig. 6 for $\chi=1.5$, $N=6$, and the same initial conditions as in Fig. 5. One notices in this case a tendency towards periodicity in the exact motion of $\mathbf{J}_E$ that appears more dramatic as one departs from the immediate vicinity of the fixed point. The characteristic times for this recurrence towards the Bloch sphere are strikingly similar (close to $6.8\hbar/\epsilon$) while the TDHF period increases from zero to infinity (extremum and separatrix, respectively).

2. Extraordinary zone

As one investigates initial conditions in this region, one can find evidences of the fact that discontinuities of the TDHF flow pattern across separatrices may not, in general, possess images in the exact dynamics. This is illustrated in Fig. 7, where we show the trajectories of the exact polarization J_E projected on the (J_x,J_z) and (J_x,J_y) planes, for the initial conditions $\theta_0=0.5\pi$, 0.53π, 0.6π, and 0.65π along the meridian $\varphi=\pi$ where the relative extrema lie. These points cover the interval of θ values between the equator and the fixed one on a given hemisphere. We can see in this figure that the exact motion is periodic and that the shape of the orbits is very similar for the various initial conditions with the deformations occurring in a continuous way. This continuity shows up, in particular, when the initial conditions lie in a small neighborhood of the equator, opposite to the TDHF case whose orbits are definitively different on either side of the equator. The periodicity here exhibited is an unexpected outcome of the numerical work and one can trace it to the peculiar phase relations among the wave function components as the motion starts both in the vicinity of the $\varphi=\pi$ meridian and of the equator.

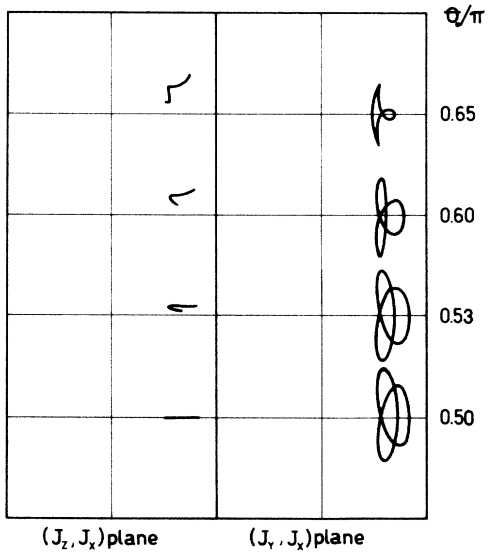

FIG. 7. The projections of the exact polarization vector on the (J_z,J_x) and (J_y,J_x) planes, respectively, for initial conditions θ_0/π along the meridian $\varphi=\pi$. The corresponding self-consistent orbits belong to the extraordinary region of phase space.

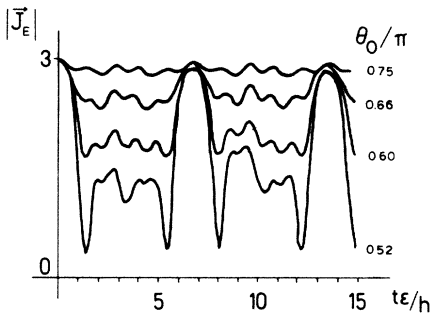

FIG. 6. Same as in Fig. 5, once the phase transition has taken place ($\chi=1.5$).

The modulus $|\mathbf{J}_E|$ of the exact polarization corresponding to an initial condition coincident with (or near to) a relative extremum does not stay in the vicinity of this point, in contrast with the evolution near extrema in the ordinary zone. However, one finds the same kind of recurrence observed in the latter region, in other words, the exact polarization approaches back the surface of the sphere with a period T close to $10\hbar/\epsilon$, almost independently of the initial condition (within the extraordinary zone), while the TDHF period varies between zero and infinity across the region.

IV. SUMMARY AND CONCLUSIONS

In this work we have examined the TDHF dynamics of a quasispin system where the parity invariance has been suppressed by an appropriate selection of the intersection. The kind of motion provided by the TDHF method has been compared to the exact dynamics for low particle number. In particular, the results here displayed correspond to $N=6$ and the features encountered and discussed are common to all particle numbers up to a few

tens, with increasing improvement of the TDHF description as compared to the exact one.

The major characteristics of the constant energy surfaces have been studied looking at the flow pattern generated by a classical Hamiltonian obtained as the expectation value of the one-plus-two-body fermion Hamiltonian. Each trajectory in the phase portrait is the intersection of an energy surface with the Bloch sphere and it is seen that a qualitative change or catastrophe, related to the well-known phase transition of the standard SU(2) model, takes place for interaction strengths $|\chi| = 1$. On the other hand, these trajectories are the integrals of the equations of motion of the one-body observables, namely the components of the quasispin vector, when their expectation values are taken with respect to a Slater determinant or coherent state. These equations are analogous to those of an incompressible geodesic flow, whose stream lines are the trajectories on the Bloch sphere. According to this image, one realizes that the velocity dJ/dt is larger in those regions with a high density of stream lines.

The comparison between approximate and exact calculations yields the following main results. First, one concludes that in order to clarify the characteristics of the evolution, it is more important to specify the zone in phase space where the initial condition lies than to point at the particular orbit where that condition belongs. In this sense, there is a kind of generic behavior inside each invariant set (topologically distinct region) of phase space. Second, the shape of the exact orbits varies in a continuous fashion with respect to the initial conditions, with characteristic recurrence times or periods almost independent of the latter.

Third, near absolute extrema the exact orbits are very localized; consequently they are very similar to the corresponding TDHF ones. The trajectories become progressively delocalized as the initial condition approaches the equator.

Finally, the present study illustrates the extent to which TDHF and exact paths differ in the neighborhood of a separatrix, since the latter is associated with a discontinuous change of topology of the TDHF orbits and a continuous variation of the exact ones.

As a final remark, we must recall that due to the nature of the original Hamiltonian, it is not possible to improve the agreement between approximate and exact dynamics or to extend the time during which the former holds, resorting to symmetry restoration as in prior works.[13,14] However, we can find that under given conditions, a proper multideterminantal trial wave function is a much better choice than a coherent state. This investigation is in progress and will be presented elsewhere.

ACKNOWLEDGMENTS

The authors are indebted to the Programa de Investigaciones en Física del Plasma (PRIFIP) at their home institution for unlimited access to their computing facilities. This work was performed under Grant No. 9413c/83 from Consejo National de Investigaciones Científicas y Técnicas (CONICET) of Argentina. Two of us (E. S. H. and H. G. S.) acknowledge the CONICET for financial support.

[1]P. Bonche, S. E. Koonin, and J. W. Negele, Phys. Rev. C **13**, 1226 (1976).
[2]H. Flocard, S. E. Koonin, and M. S. Weiss, Phys. Rev. C **17**, 1681 (1978).
[3]H. Flocard, Nucl. Phys. **A387**, C283 (1982).
[4]K. T. R. Davies, K. R. S. Devi, S. E. Koonin, and M. R. Strayer, Marmal Aid Report MAP-23, 1982 (unpublished).
[5]J. M. Irvine, Comput. Phys. Commun. **26**, 433 (1982).
[6]J. W. Negele, Rev. Mod. Phys. **54**, 913 (1982).
[7]P. C. Lichtner and J. J. Griffin, Phys. Rev. Lett. **37**, 1521 (1976).
[8]Da Hsuan Feng and R. Gilmore, Phys. Lett. **90B**, 327 (1980).
[9]R. Gilmore, J. Math. Phys. **20**, 891 (1979).
[10]H. G. Solari and E. S. Hernández, Z. Phys. A **321**, 155 (1985).
[11]S. J. Krieger, Nucl. Phys. **A276**, 12 (1977).
[12]H. G. Solari and E. S. Hernández, Phys. Rev. C **26**, 2310 (1982).
[13]H. G. Solari and E. S. Hernández, Phys. Rev. C **28**, 2472 (1983).
[14]H. G. Solari and E. S. Hernández, Phys. Rev. C **32**, 462 (1985).
[15]H. J. Lipkin, N. Meshkov, and A. J. Glick, Nucl. Phys. **62**, 188 (1965).
[16]E. S. Hernández and D. M. Jezek (unpublished).
[17]R. Gilmore and D. H. Feng (unpublished).
[18]K. K. Kan, P. C. Lichtner, M. Dworzecka, and J. J. Griffin, Phys. Rev. C **21**, 1098 (1980).
[19]K. K. Kan, Phys. Rev. C **22**, 2228 (1980).
[20]R. Gilmore and D. H. Feng, Nucl. Phys. **A301**, 189 (1978).
[21]F. T. Arecchi, E. Courtens, R. Gilmore, and H. Thomas, Phys. Rev. A **6**, 2211 (1972).
[22]R. Gilmore, Rev. Mex. Fis. **23**, 143 (1974).
[23]P. A. M. Dirac, Proc. Cambridge Philos. Soc. **26**, 376 (1930).
[24]D. J. Rowe, A. Ryman, and G. Rosensteel, Phys. Rev. A **22**, 2362 (1980).
[25]K. K. Kan, J. G. Griffin, P. C. Lichtner, and M. Dworzecka, Nucl. Phys. **A332**, 109 (1979).
[26]V. J. Arnold, *Mathematical Methods of Classical Mechanics* (Springer, New York, 1978).